A Novel *KCNQ1* Missense Mutation Identified in a Patient with Juvenile-Onset Atrial Fibrillation Causes Constitutively Open I_{Ks} Channels

Kanae Hasegawa, MD,[*,†] Seiko Ohno, MD, PhD,[†] Takashi Ashihara, MD, PhD,[†]

Hideki Itoh, MD, PhD,[†] Wei-Guang Ding, PhD,[‡] Futoshi Toyoda, PhD,[‡]

Takeru Makiyama, MD, PhD,[§] Hisaaki Aoki, MD, PhD,[¶]

Yoshihide Nakamura, MD, PhD,[¶] Brian P. Delisle, PhD, [#]

Hiroshi Matsuura, MD, PhD,[‡] Minoru Horie, MD, PhD,[†]

[*] Department of Cardiovascular Biology and Medicine, Niigata University School of Medical and Dental Sciences, Niigata, Japan.

[†] Department of Cardiovascular and Respiratory Medicine, Shiga University of Medical Science, Otsu, Japan.

[‡] Department of Physiology, Shiga University of Medical Science, Otsu, Japan.

[§] Department of Cardiovascular and Medicine, Kyoto University Graduate School of Medicine, Kyoto, Japan.

[¶] Department of Pediatrics, Kinki University Faculty Medicine, Osaka, Japan.

[#] Department of Physiology, University of Kentucky, Lexington, USA.

Running title: **A novel *KCNQ1* mutation in Juvenile-Onset AF**

Total words count: 4979 words

This work was supported by Grants-in-Aid in Scientific Research from the Ministry of Education, Culture, Science, and Technology of Japan, a Health Sciences Research Grant from the Ministry of Health, Labour and Welfare of Japan, and Translational Research Funds from the Japan Circulation Society.

There are no conflicts of interest for all authors.

Address for correspondence: Minoru Horie MD, PhD, Department of Cardiovascular and Respiratory Medicine, Shiga University of Medical Science, Seta Tsukinowa-cho, Otsu 520-2192, Japan

Tel: +81-77-548-2213, **Fax**: +81-77-543-5839

E-Mail: horie@belle.shiga-med.ac.jp

Abstract

Background: Atrial fibrillation (AF) is one of the most common cardiac arrhythmias, and in some patients, the disease is inheritable. Hereditary aspects of AF, however, remain not fully elucidated.

Objective: The purpose of this study was to identify genetic backgrounds contributed to juvenile-onset AF and to define the mechanism.

Methods: In 30 consecutive juvenile-onset AF patients (onset age <50 year-old), we screened AF-related genes (*KCNQ1, KCNH2, KCNE1-3* and *5, KCNJ2,* and *SCN5A*). We analyzed the function of mutant channels using whole-cell patch-clamp techniques and computer simulations.

Results: Among the juvenile-onset AF patients, we identified three mutations (10%), *SCN5A*-M1875T, *KCNJ2*-M301K, and *KCNQ1*-G229D. Since *KCNQ1* variant (G229) identified in a 16-year-old boy was novel, we focused on the proband. The G229D-I_{Ks} was found to induce a large instantaneous activating component without deactivation after repolarization to –50 mV. In addition, WT/G229D-I_{Ks} (WT and mutant co-expression) displayed both instantaneous and time-dependent activating currents. Compared to WT-I_{Ks}, the tail current densities in WT/G229D-I_{Ks} were larger at test potentials between –130 and –40 mV, but smaller at test potentials between 20 and 50 mV. Moreover, WT/G229D-I_{Ks} resulted in a negative voltage shift for current activation (−35.2 mV) and slower deactivation. WT/G229D-I_{Ks} conducted a large outward current

induced by an atrial action potential waveform, and computer simulation incorporating the WT/G229D-I_{Ks} results revealed that the mutation shortened atrial but not ventricular action potential.

Conclusion: A novel *KCNQ1*-G229D mutation identified in a juvenile-onset AF patient altered the I_{Ks} activity and kinetics, thereby increasing the arrhythmogenicity to AF.

Key words:

atrial fibrillation; juvenile-onset atrial fibrillation; ion channel; I_{Ks}; KCNQ1

Abbreviations:

AF = atrial fibrillation,

AP = action potential,

CHO cell = Chinese hamster ovary cell,

ECG = electrocardiogram,

HR = heart rate,

QTc = corrected QT interval.

Introduction

Atrial fibrillation (AF) is the most prevalent cardiac rhythm abnormality and one of the major cause of morbidity and mortality [1]. There are many risk factors predisposing to AF: advancing age, male sex, structural heart disease, hypertension, obesity, diabetes mellitus, and hyperthyroidism [1]. In some patients, AF occurs in the absence of these risk factors, and this subtype is called as lone AF [2]. Genetic backgrounds have been shown to be associated with lone AF [3]. In fact, mutations in genes encoding ion channels [4-11], gap junction proteins [12], and signaling molecules [13] have been identified in families with AF and isolated AF cases [14]. Among these AF-related genes, in 2003, Chen and his colleagues first revealed the link between AF and a *KCNQ1* mutation (a gene encodes the slowly activating component of delayed rectifier K^+ current (I_{Ks})) [4]. They reported a missense *KCNQ1* mutation, S140G, in familial AF, which showed a gain-of-function effect of I_{Ks} [4, 15].

To date, seven *KCNQ1* mutations have been reported to be associated with AF by exerting a gain-of-function effect with enhanced I_{Ks} current density with or without altered gating [4, 16-21]. And five of seven *KCNQ1* mutations, S140G, V141M, S209P, R231C, and R231H were identified in juvenile-onset AF patients. Among these five mutations, S140G, R231C, and R231H mutations were associated with QT prolongation. Regarding other mutations in genes that encode ion channels, functional analyses of the mutations have demonstrated either gain-of-function effects, for example in *SCN5A* and

KCNJ2 [5, 6] or loss-of-function effects in *SCN5A* and *KCNA5* [10, 11]. Intriguingly, these functional alterations are similar to those found in the electrophysiological remodeling in chronic AF [22].

In order to clarify the genetic basis of juvenile-onset AF, we screened 30 consecutive probands for mutations in *KCNQ1, KCNH2, KCNE1-3* and *5, KCNJ2,* and *SCN5A*. Three heterozygous mutations were identified in *SCN5A*, *KCNJ2*, and *KCNQ1* in three probands from unrelated families (10 %). We have reported the former two mutations, *SCN5A*-M1875T and *KCNJ2*-M301K [5, 6]. The third missense *KCNQ1* mutation, G229D, was identified in a 16-year-old boy with AF and it is novel. We examined the molecular mechanism underlying the *KCNQ1* mutation found in juvenile-onset AF by using a heterologous expression. We then incorporated the functional impact of the mutation into computational simulations of the atrial action potential (AP), and we found that it could contribute to the shortening of the atrial AP duration, leading to the arrhythmogenicity of AF.

Methods

Study subjects

The present study was approved by the Institutional Ethics Committees of our institutes, and all patients provided informed consent. Thirty consecutive AF probands who developed AF at age of <50 year-old were included in this study.

DNA Isolation and Genetic Analysis

Genomic DNA was isolated from blood lymphocytes and screened for the entire open reading frames of *KCNQ1, KCNH2, KCNE1-3* and *5, KCNJ2,* and *SCN5A*. Genetic screening (except for *KCNJ2*) was performed using denaturing high-performance liquid chromatography (dHPLC WAVE System; Transgenomic, Omaha, NE, USA). Abnormal conformers and *KCNJ2* were amplified via PCR, and sequencing was performed on ABI PRISM3130 DNA sequencer (Applied Biosystems, Wellesley, MA, USA). When a mutation was detected, we examined its presence in >200 Japanese healthy individuals to exclude the possibility of polymorphisms. When a mutation was detected in a proband, we checked whether or not their family members were also carriers.

In Vitro Mutagenesis

Full-length cDNA encoding human wild-type (WT) KCNQ1 (GenBank AF000571) in a pCI vector, was subcloned into a pIRES2-EGFP expression vector. We engineered *KCNQ1*-G229D mutant using a site-directed mutagenesis kit, QuikChange II XL (Stratagene, La Jolla, CA, USA). The presence of mutations was confirmed by sequencing. Full-length cDNA encoding human KCNE1 (GenBank M26685) subcloned into the pCDNA3.1 expression vector was obtained by PCR from human heart cDNA

library (Clontech Laboratories, Inc. CA, USA).

Electrophysiological Experiments

To assess the functional modulation by *KCNQ1* mutation, we used a heterologous expression system with the Chinese Hamster Ovary (CHO) cell line. Briefly, the cells were transiently transfected with *KCNQ1*-WT (0.5 μg) or *KCNQ1*-G229D (0.5 μg) or *KCNQ1*-WT (0.25 μg)/G229D (0.25 μg), and *KCNE1* (0.5 μg) plasmid DNA using Lipofectamine (Invitrogen Life Technologies, Inc. Carlsbad, CA, USA). For electrophysiological experiments, after 48 hours transfection, cells attached to glass coverslips were transferred to a 0.5 ml bath chamber perfused with extracellular solution at 1-2 ml/min. The chamber was mounted on the stage of an inverted microscope (ECLIPSE TE2000-U, Nikon, Tokyo, Japan) and maintained at 37°C. Patch-clamp experiments were conducted on GFP-positive cells.

Whole-cell membrane currents were recorded with an EPC-8 patch-clamp amplifier (HEKA Electronik, Lambrecht, Germany). Pipettes were prepared from glass capillary tube (Narishige, Tokyo, Japan) by mean of a Sutter P-97 micropipette puller (Navato, CA, USA), and the tips were then fire-polished with a microforge. Pipette resistance ranged from 2.5-3.5 MΩ. Pipettes were filled with a solution containing (mM): 70 potassium aspartate, 40 KCl, 10 KH_2PO_4, 1 $MgSO_4$, 3 Na_2-ATP (Sigma), 0.1 Li_2-GTP (Roche Diagnostics GmbH, Mannheim, Germany), 5 EGTA and 5 HEPES, and pH was

adjusted to 7.2 with KOH. The extracellular solution contained (mM): 140 NaCl, 5.4 KCl, 1.8 $CaCl_2$, 0.5 $MgCl_2$, 0.33 NaH_2PO_4, 5.5 glucose and 5.0 HEPES, and pH was adjusted to 7.4 with NaOH. Liquid junction potential between the test solution and the pipette solution was measured to be around –10 mV and was corrected. HMR1556 (a kind gift from Drs. H.J. Lang and J. Punter, Aventis Pharma Deutschland GmbH), a selective I_{Ks} blocker, was added from 10 mM stock solution in DMSO to the external solution (final DMSO concentration did not exceed 0.01%).

I_{Ks} was elicited by depolarizing voltage steps from holding potential of –80 mV to various test potentials. I_{Ks} amplitude was determined by measuring the amplitude of tail current elicited upon repolarization to –50 mV following 2-s depolarization to 30 mV every 15 s and divided by the cell membrane capacitance to obtain current densities (pA/pF). I_{Ks} activation was evaluated by fitting the current-voltage relationship of the tail currents to a Boltzmann equation:

$$I_{\mathrm{Ktail}} = 1\Big/\left(1+\exp\left(\left(V_{\mathrm{h}}-V_{\mathrm{m}}\right)/k\right)\right),$$

where I_{Ktail} is the current amplitude density, V_{h} is the voltage at half-maximal activation, V_{m} is the test potential and k is the slope factor. Time constants for deactivation ($\mathrm{tau}_{\mathrm{fast}}$ and $\mathrm{tau}_{\mathrm{slow}}$) were obtained by fitting a two-exponential function shown below:

$$I(\mathrm{t}) = A_{\mathrm{fast}}\exp\left(-t/\mathrm{tau}_{\mathrm{fast}}\right) + A_{\mathrm{slow}}\exp\left(-t/\mathrm{tau}_{\mathrm{slow}}\right) + A_0,$$

where I(t) means the current amplitude at time t, A_{fast}, A_{slow} and A_0 are constants, and τ refers to the deactivation at the tail potential.

For voltage-clamp recordings using an atrial AP waveform, we applied a waveform generated from a computer simulation of an atrial AP at 1 Hz and recorded currents at 37°C [21].

Resting membrane potential in CHO cell was determined by current-clamp after creating the whole-cell configuration.

Computer simulation

To confirm the role of the *KCNQ1*-G229D mutation, we conducted simulations of paced activation in atrial and ventricular myocytes and of paced propagation in a one-dimensional (1D) bidomain ventricular myocardial model of 9.0-mm length with transverse conductivity, mimicking transmural section of left ventricular free wall. Membrane kinetics of the myocytes were represented by Courtemanche human atrial model [23] and O'Hara-Rudy human ventricular model [24], of which I_{Ks} models were replaced by the following equations based upon WT-I_{Ks} or WT/G229D-I_{Ks} obtained in electrophysiological recordings.

For both WT-I_{Ks} and WT/G229D-I_{Ks}:

$$I_{Ks} = G_{Ks} \cdot \left(1 + 0.6 / \left(1 + \left(3.8 \cdot 10^{-5} / [Ca^{2+}]_i\right)^{1.4}\right)\right) \cdot x_{s1} \cdot x_{s2} \cdot \left(V_m - E_{Ks}\right),$$

$$dx_{s1} / dt = \left(x_{s,\infty} - x_{s1}\right) / tau_{x,s1},$$

$$dx_{s2} / dt = \left(x_{s,\infty} - x_{s2}\right) / tau_{x,s2},$$

For WT-I_{Ks}:

$$x_{s,\infty} = 1/\left(1+\exp\left(-\left(V_m+28.8\right)/15.45\right)\right),$$

$$\mathrm{tau}_{x,s1} = 326.9+0.4/\left(2.326\cdot10^{-4}\cdot\exp\left(\left(V_m+65.5\right)/17.8\right)+1.292\cdot10^{-3}\cdot\exp\left(-\left(V_m+227.2\right)/230\right)\right),$$

$$\mathrm{tau}_{x,s2} = 5/\left(0.01\cdot\exp\left(\left(V_m-50\right)/100\right)+0.0193\cdot\exp\left(-\left(V_m+66.54\right)/155\right)\right),$$

For WT/G229D-I_{Ks}:

$$x_{s,\infty} = 0.85/\left(1+\exp\left(-\left(V_m+82.8\right)/41.72\right)\right),$$

$$\mathrm{tau}_{x,s1} = 326.9+0.4/\left(2.326\cdot10^{-4}\cdot\exp\left(\left(V_m+119.5\right)/17.8\right)+1.292\cdot10^{-3}\cdot\exp\left(-\left(V_m+281.2\right)/230\right)\right),$$

$$\mathrm{tau}_{x,s2} = 5/\left(0.01\cdot\exp\left(\left(V_m-50\right)/100\right)+0.0193\cdot\exp\left(-\left(V_m+66.54\right)/155\right)\right),$$

where G_{Ks} (mS/μF) is the maximum conductance of I_{Ks}; $[Ca^{2+}]_i$ (mM) is the intracellular Ca^{2+} concentration; x_{s1} and x_{s2} are the activation and deactivation gates, respectively, for I_{Ks}; V_m (mV) is the transmembrane potential; E_{Ks} (mV) is the reversal potential for I_{Ks}; $x_{s,\infty}$ is the steady-state value of both x_{s1} and x_{s2} gates; and $\mathrm{tau}_{x,s1}$ and $\mathrm{tau}_{x,s1}$ are the time constant of x_{s1} and x_{s2} gates, respectively. The values of G_{Ks} for atrial and ventricular models were 0.0136 and 0.0034 mS/μF, respectively, because the WT-I_{Ks} with these values faithfully reproduced the same current amplitudes as in the original I_{Ks} models [23, 24].

To obtain the ventricular transmural gradient, we defined endocardial, mid-myocardial, and epicardial layers of thicknesses, 0.6 mm, 6.0 mm, and 2.4 mm, respectively [25], and then we incorporated transmural differences in ion channels and intracellular Ca^{2+} dynamics according to the original code [24]. Pacing stimuli of 2-ms duration and strength twice-diastolic threshold were applied transmembranously to the

endocardial end at a cycle length of 1000 ms. To obtain electrocardiograms (ECG) similar to those recorded from left precordial leads, a unipolar recording electrode was located 2 cm above the epicardial end of the tissue. Transmural conductivity in the extracellular space was set to 2.36 mS/cm, and that in the intracellular space for endocardial and mid-myocardial layers and for epicardial layer were set to 0.38 and 0.29 mS/cm, respectively [26]. Other model parameters and the numerical approach have been described elsewhere [25].

Statistical Analysis

All the data are shown as mean ± standard error of the mean (SEM). Differences between two groups were examined by Independent Student's t-test. A value of $p < 0.05$ was considered significant.

Results

Genetic analysis

We identified 3 heterozygous mutations in 3 of 30 probands with juvenile-onset AF (10 %): *SCN5A*-M1875T, *KCNJ2*-M301K and *KCNQ1*-G229D. Details of patients with *SCN5A*-M1875T and *KCNJ2*-M301K have been reported previously [5, 6]. The third *KCNQ1* mutation, a single-base substitution at nucleotide 686 (c.686G>A), causes an amino acid change from glycine to aspartic acid at position 229 in the Kv7.1 potassium

channel (Fig. 1A). Gly-229 resides in the fourth transmembrane segment (S4), which is known as a voltage sensor (Fig. 1B). Alignment of the Kv7.1 amino acid sequence (Fig. 1C) demonstrated that the glycine at position 229 is conserved in several species, suggesting its importance at this position. G229D was absent in 400 Japanese control alleles and have not been reported according to the NHLBI Exome Sequencing Project (ESP), Exome Variant Server (http://evs.gs.washington.edu/EVS/).

In the proband, we did not find any mutations in other candidate genes described in the methods.

Clinical Characteristics

KCNQ1-G229D mutation was identified in a 16-year-old boy, who was diagnosed as AF at the age of 16 (Fig. 2A, QT/QTc, 380/429 ms). Cardiovascular and blood examination including thyroid hormone were all normal. He took propranolol hydrochloride (30 mg/day) and digoxin (0.125 mg/day) for the purpose of rate control and bepridil (100 mg/day) for pharmacological cardioversion, but failed to maintain his sinus rhythm. Moreover cardioversion did not restore sinus rhythm.

As the next step for treatment, he received radiofrequency catheter ablation therapy (pulmonary vein isolation). After the therapy, his AF did not recur without any antiarrhythmic agents for 20 months. Eighteen months after therapy, exercise tolerance test was performed (Fig. 2B). The QTc interval at both rest and 4 min recovery after

exercise showed borderline criteria of QT prolongation (QT/QTc, from 415/452 ms to 372/480 ms).

The G229D mutation was also identified in his asymptomatic mother, and her ECG at rest showed borderline criteria of QT prolongation (QT/QTc, 460/468 ms) (Fig. 2C), and there was no family history of AF (Fig. 2D).

Functional Analysis

To elucidate the genetic effect of G229D mutant, we conducted functional characterization by using a heterologous expression system. As shown in Figure 3A, co-expression of *KCNQ1*-WT (0.5 μg) with *KCNE1* (0.5 μg) produced a slowly activating outward WT-I_{Ks} upon depolarization to 30 mV from the holding potential of –80 mV. In contrast, the transfection of *KCNQ1*-G229D (0.5 μg), co-expressed with equimolar *KCNE1*, produced an instantaneously activated G229D-I_{Ks} that did not deactivate after repolarization to –50 mV (Fig. 3B). Moreover, the cells co-expressing WT and mutant (0.25 μg, each) channels with *KCNE1* displayed both instantaneous (indicated by an arrow) and time-dependent activated WT/G229D-I_{Ks} with deactivation process (Fig. 3C), suggesting that the co-expression of WT results in an intermediate functional phenotype. HMR 1556 (an I_{Ks} blocker; 1 μM) completely inhibited all conducted-I_{Ks} currents (indicated by red traces in Fig. 3A-C).

Activating currents were then divided into instantaneous and time-dependent

components, by measuring the instantaneous current level at 10 ms after depolarization pulse and the time-dependent current as a difference between current level at 10 ms after depolarization and at the end of depolarizing duration (steady-state: indicated by an arrow head in Fig. 3C). As summarized in bar graphs of Figure 3D, instantaneous components of WT/G229D-I_{Ks} were 171.9±28.3 pA/pF, which was significantly larger than those in WT-I_{Ks} (40.8±14.1 pA/pF, $p<0.001$). In contrast, time-dependent and steady-state currents were significantly larger in WT-I_{Ks} than WT/G229D-I_{Ks} (Fig. 3C & D).

Figures 4A depicts two families of I_{Ks} current traces elicited by 2-s depolarizing voltage-clamp steps, from a holding potential of –80 mV, to various test potentials and following repolarization to –50 mV (inset shows the voltage-step protocol): left, WT-I_{Ks} and right, WT/G229D-I_{Ks}. Again, WT/G229D-I_{Ks} displayed an instantaneous activation (indicated by an arrow in Fig. 4A), which was followed by time-dependent slow activation (intermediate phenotype). On repolarization to –50 mV, tail currents did not completely deactivate. As shown in the lower panels, both WT and WT/G229D currents were entirely inhibited by HMR1556 (1 μM).

Figures 4B shows peak tail current-voltage relationships for WT-I_{Ks} and WT/G229D-I_{Ks} obtained from multiple experiments. Tail current densities were larger at test potentials between –130 and –40 mV in WT/G229D (filled circles) than WT (open circles). At more depolarizing test pulses (20 to 50 mV), however, they were

reversely smaller in WT/G229D than WT.

In Figure 4C, voltage-dependent activations of WT and WT/G229D tail currents were evaluated by fitting to a Boltzmann equation. In WT/G229D, the voltage dependence for I_{Ks} activation was significantly shifted to more hyperpolarized potentials (from –15.1±1.4 to –50.8±7.8 mV).

Because deactivation of WT/G229D-I_{Ks} was extremely slow at –50 mV (Fig. 3C & 4A), in the following experiments (Fig. 5A), we measured deactivation kinetics (tau_{fast} and tau_{slow}) at –120 mV after 2-s depolarization to 30 mV (WT: left trace and WT/G229D: right trace). As summarized in bar graphs of Figure 5B, compared to WT, rates for deactivation in WT/G229D were significantly slower (tau_{fast}, 77.3±3.6 ms vs. 115.0±8.9 ms; tau_{slow}, 270.9±124.9 ms vs. 1716.3±110.9 ms).

In the next series of experiments, we employed an atrial AP waveform to elicit the current activation. WT/G229D-I_{Ks} thus conducted large outward currents (red trace: Fig. 6A). As summarized in bar graphs of Figure 6B, integral current densities were significantly larger in WT/G229D than WT, suggesting a gain-of-function effect by G229D mutation.

Since the instantaneous current component of WT/G229D-I_{Ks} could influence the resting membrane potential, we then measured the resting potential of CHO cells expressing various constructs (Fig. 6C). Resting membrane potentials were –4.6±1.9 mV in non-transfected cells and were –41.3±2.2 mV in cells expressing WT channels.

In contrast, those expressing WT/G229D or G229D channels showed significantly more negative resting potentials (–74.6±1.9 mV and –74.3±6.2 mV), which were closer to the calculated equilibrium potential of potassium ion (–89.9 mV in the present experimental condition). Therefore the negative shift of resting potentials may be due to the constitutive opening of WT/G229D or G229D channels.

Computer simulation

To explore the cellular mechanisms by which the G229D mutation manifested AP shortening in atrial but not ventricular myocytes, we performed a computer simulation study by employing both atrial and ventricular myocyte and 1D myocardial model (Fig. 7). Based on the I_{Ks} obtained in the electrophysiological recording (Figs. 4 & 5), we numerically reproduced both WT and WT/G229D current traces (Fig. 7A), the current-voltage relationship curves (Fig. 7B), and the normalized activation curves (Fig. 7C). The numerically-reproduced I_{Ks} were incorporated into the human atrial and ventricular myocyte models (Fig.7D & E, respectively). WT/G229D-I_{Ks} was markedly larger than WT-I_{Ks} in both atrial and ventricular cell models. Because of the difference in the contribution of I_{Ks} to the AP formation, the mutation markedly shortened the AP duration in the atrial but not ventricular myocyte model. Indeed, the numerically-reproduced I_{Ks} did not shorten the QT interval in the 1D model under 1 Hz pacing (Fig. 7F), consistent with the ECG phenotype of the proband.

Discussion

In the present study, we described a novel missense *KCNQ1* mutation, G229D, in a juvenile-onset AF patient. The proband's AF started at the age of 16, which was refractory to bepridil. Radiofrequency catheter ablation therapy was effective to maintain his sinus rhythm. In sinus rhythm, he showed borderline QT prolongation. His mother carried the same heterozygous mutation and also showed borderline QT prolongation.

G229D mutant I_{Ks} reconstituted in CHO cells displayed unique functional properties: time-independent component (instantaneous current) and slow deactivation. In detail, (1) instantaneous component of WT/G229D was significantly larger than that of WT; (2) the tail current density of WT/G229D was larger at test potentials between –130 and –40 mV; (3) WT/G229D produced a negative shift in the voltage-dependence of half maximal activation (–35.2 mV); (4) the deactivation of WT/G229D was significantly slower than that of WT; (5) a large integral current density of WT/G229D was indeed induced by the atrial AP clamp experiment; and (6) computational AP simulations suggest WT/G229 selectively shortens the atrial AP. Taken together, these results are consistent with a view that the mutation caused gain-of-function effects on $I_{Ks,}$ thereby shortening atrial refractoriness and increasing susceptibility to AF.

Regarding *KCNQ1* mutations associated with juvenile-onset AF, five mutations, S140G, V141M, S209P, R231C, and R231H, were previously identified [4, 16, 19-21].

Chen et al. [4] first reported that *KCNQ1*-S140G mutation which potentiated $I_{Ks,}$ especially the component of instantaneous activation. Later in 2005, Hong et al. [16] reported *KCNQ1*-V141M mutation in a baby with AF and an abnormally short QT interval. They also described a large instantaneous activation of V141M-I_{Ks}. Then, Das et al. [19] reported a heterozygous *KCNQ1*-S209L mutation. This mutation also showed an instantaneous opening when expressed as WT/S209L-I_{Ks}, a significantly negative shift of half maximal activation voltage (–42.4 mV), and slow current deactivation.

More recently, Bartos et al. [20, 21] reported *KCNQ1*-R231C and R231H mutations in families with AF and mild QT prolongation. These mutations showed marked instantaneous activation and significantly negative shift in half maximal activation (–30 to –40 mV). In addition, recent extensive mutagenesis experiments and the structural model of KCNQ1 protein [15] suggest residues S140, E160, R237, and R231 closely associate with one another in the closed state. Substitution of amino acid at either of charged S140, E160, R237, or R231 residues was shown to disrupt KCNQ1 deactivation ("lock" the I_{Ks} channel in the open state) [15, 20]. This suggests that these residues are critical for normal KCNQ1 channel closing and that G229D might also disrupt the interaction among these residues.

Our biophysical assessment revealed that the function of G229D resembled that of R231C and R231H mutations [20, 21], which resides near glycine at 229. However, the G229D mutation was somewhat different in that it caused a borderline QT prolongation.

Indeed, it appeared not to affect the ventricular AP while markedly shortening the atrial AP. Our computer simulation 1D model (Fig. 7F) partially explained these apparently different effects of G229D for the first time. Regarding the pharmacological treatment of AF in the proband, a low concentration of pure I_{Ks} blocker would be a potential to restore sinus rhythm without considerable prolongation of QT interval. In fact, Courtney et al. [27] recently reported the enhanced sensitivity of *KCNQ1* gain-of-function mutation (S140G) for HMR-1556, a pure I_{Ks} blocker, compared to that of WT channels.

Study limitations

In the present study, we employed a heterologous expression system to assess the functional modulation by the *KCNQ1* mutation. However, the environment of this system is different from that of cardiac myocytes or whole heart. Therefore, our data might not always explain the electrophysiological modulation in the whole heart.

Conclusion

We identified a novel *KCNQ1*-G229D mutation in a juvenile-onset AF patient. In the heterozygous condition, the mutation changed I_{Ks} channel kinetics and showed a gain-of-function modulation of I_{Ks}. In the computer simulation model, it markedly shortened the atrial AP duration, suggesting the tendency to AF.

Acknowledgment

The authors are grateful to the Japanese juvenile-onset AF families for their willingness to participate in this study. We thank Dr. Daniel C. Bartos (Department of Physiology, University of Kentucky, Lexington, USA) for the AP waveform and Arisa Ikeda, Kazu Toyooka, and Aya Umehara for excellent technical assistance.

References

[1] Kannel WB, Benjamin EJ: Status of the epidemiology of atrial fibrillation. Med Clin North Am 2008;92:17-40, ix.

[2] Brand FN, Abbott RD, Kannel WB, Wolf PA: Characteristics and prognosis of lone atrial fibrillation. 30-year follow-up in the Framingham Study. JAMA 1985;254:3449-3453.

[3] Sinner MF, Ellinor PT, Meitinger T, Benjamin EJ, Kaab S: Genome-wide association studies of atrial fibrillation: past, present, and future. Cardiovasc Res 2011;89:701-709.

[4] Chen YH, Xu SJ, Bendahhou S, et al: KCNQ1 gain-of-function mutation in familial atrial fibrillation. Science 2003;299:251-254.

[5] Makiyama T, Akao M, Shizuta S, et al: A novel SCN5A gain-of-function mutation M1875T associated with familial atrial fibrillation. J Am Coll Cardiol 2008;52:1326-1334.

[6] Hattori T, Makiyama T, Akao M, et al: A novel gain-of-function KCNJ2 mutation associated with short-QT syndrome impairs inward rectification of Kir2.1 currents. Cardiovasc Res 2012;93:666-673.

[7] Ravn LS, Aizawa Y, Pollevick GD, et al: Gain of function in IKs secondary to a mutation in KCNE5 associated with atrial fibrillation. Heart Rhythm 2008;5:427-435.

[8] Lundby A, Ravn LS, Svendsen JH, Hauns S, Olesen SP, Schmitt N: KCNE3 mutation V17M identified in a patient with lone atrial fibrillation. Cell Physiol Biochem 2008;21:47-54.

[9] Yang Y, Xia M, Jin Q, et al: Identification of a KCNE2 gain-of-function mutation in patients with familial atrial fibrillation. Am J Hum Genet 2004;75:899-905.

[10] Ellinor PT, Nam EG, Shea MA, Milan DJ, Ruskin JN, MacRae CA: Cardiac sodium channel mutation in atrial fibrillation. Heart Rhythm 2008;5:99-105.

[11] Olson TM, Alekseev AE, Liu XK, et al: Kv1.5 channelopathy due to KCNA5 loss-of-function mutation causes human atrial fibrillation. Hum Mol Genet 2006;15:2185-2191.

[12] Gollob MH, Jones DL, Krahn AD, et al: Somatic mutations in the connexin 40 gene (GJA5) in atrial fibrillation. N Engl J Med 2006;354:2677-2688.

[13] Hodgson-Zingman DM, Karst ML, Zingman LV, et al: Atrial natriuretic peptide frameshift mutation in familial atrial fibrillation. N Engl J Med 2008;359:158-165.

[14] Mahida S, Lubitz SA, Rienstra M, Milan DJ, Ellinor PT: Monogenic atrial fibrillation as pathophysiological paradigms. Cardiovasc Res 2011;89:692-700.

[15] Restier L, Cheng L, Sanguinetti MC: Mechanisms by which atrial fibrillation-associated mutations in the S1 domain of KCNQ1 slow deactivation of IKs channels. J Physiol 2008;586:4179-4191.

[16] Hong K, Piper DR, Diaz-Valdecantos A, et al: De novo KCNQ1 mutation

responsible for atrial fibrillation and short QT syndrome in utero. Cardiovasc Res 2005;68:433-440.

[17] Lundby A, Ravn LS, Svendsen JH, Olesen SP, Schmitt N: KCNQ1 mutation Q147R is associated with atrial fibrillation and prolonged QT interval. Heart Rhythm 2007;4:1532-1541.

[18] Otway R, Vandenberg JI, Guo G, et al: Stretch-sensitive KCNQ1 mutation A link between genetic and environmental factors in the pathogenesis of atrial fibrillation? J Am Coll Cardiol 2007;49:578-586.

[19] Das S, Makino S, Melman YF, et al: Mutation in the S3 segment of KCNQ1 results in familial lone atrial fibrillation. Heart Rhythm 2009;6:1146-1153.

[20] Bartos DC, Duchatelet S, Burgess DE, et al: R231C mutation in KCNQ1 causes long QT syndrome type 1 and familial atrial fibrillation. Heart Rhythm 2011;8:48-55.

[21] Bartos DC, Anderson JB, Bastiaenen R, et al: A KCNQ1 Mutation Causes a High Penetrance for Familial Atrial Fibrillation. J Cardiovasc Electrophysiol 2012.

[22] Bosch RF, Nattel S: Cellular electrophysiology of atrial fibrillation. Cardiovasc Res 2002;54:259-269.

[23] Courtemanche M, Ramirez RJ, Nattel S: Ionic mechanisms underlying human atrial action potential properties: insights from a mathematical model. Am J Physiol 1998;275:H301-321.

[24] O'Hara T, Virag L, Varro A, Rudy Y: Simulation of the undiseased human cardiac ventricular action potential: model formulation and experimental validation. PLoS Comput Biol 2011;7:e1002061.

[25] Tsuji-Wakisaka K, Akao M, Ishii TM, et al: Identification and functional characterization of KCNQ1 mutations around the exon 7-intron 7 junction affecting the splicing process. Biochim Biophys Acta 2011;1812:1452-1459.

[26] Yamada KA, Kanter EM, Green KG, Saffitz JE: Transmural distribution of connexins in rodent hearts. J Cardiovasc Electrophysiol 2004;15:710-715.

[27] Campbell CM, Campbell JD, Thompson CH, Vanoye CG, George AL, Jr.: Selective Targeting of Gain-of-function KCNQ1 Mutations Predisposing to Atrial Fibrillation. Circ Arrhythm Electrophysiol 2013 (in press).

Figure Legends

Figure 1. ***Genetic Analysis of the proband.***

A. Electropherograms of *KCNQ1* gene showing a mutation, p.G229D (c.686G>A) in the proband. **B.** Topology of Kv7.1 encoded by *KCNQ1*. G229 is located in the fourth transmembrane segment (S4), known as voltage sensor. **C.** Alignment of Kv7.1 sequence showing the conservation of glycine at position 229 (G229) across species.

Figure 2. ***Clinical Characteristics.***

Twelve-lead electrocardiograms (ECG) of the proband, indicating atrial fibrillation at the first detection **(A)** and sinus rhythm at rest and during exercise tolerance test after catheter ablation **(B)**. **C.** ECG of his mother. **D.** Pedigree and ECG (V5 lead) of his father. Males and female were represented as squares and circle, respectively. Arrow indicates a proband. +/– symbols indicate the presence/absence of the *KCNQ1*-G229D variant. Filled symbols indicate the development of AF.

Figure 3. ***G229D mutation drastically alters properties of reconstituted I_{Ks} current.***

Whole-cell Kv7.1 currents recorded from CHO cells expressing WT **(A)**, G229D **(B)**, and WT/G229D **(C)**. Current were elicited by 2-s voltage step from a holding potential of −80 mV to 30 mV before (black trace) and after (red trace) application of HMR 1556 (1 μM). Blue lines indicate the zero current level. Inset to the lower right of panel shows

voltage application protocol.

D. Bar graphs of current densities summarized from multiple experiments for instantaneous (left), time-dependent (middle) and steady-state (right) currents during voltage step to 30 mV. Instantaneous current level was measured at 10 ms after depolarization (arrow). Time-dependent current was estimated as a difference between an instantaneous current level (arrow) and that at the end of depolarizing pulse (steady-state: arrow head). White bars indicate data from WT (n=19) and black bars those from WT/G229D (n=19).

Figure 4. ***Electrophysiologic properties of WT and WT/G229D.***

A. Representative two sets of current traces recorded from CHO cells expressing WT (left) and WT/G229D (right). Currents were elicited by 2-s depolarizing voltage-clamp steps, from a holding potential of –80 mV, to various test potentials (from –140 to 50 mV), before (upper) and after (bottom) application of HMR 1556 (1 μM). An arrow in the right panel indicates the instantaneous current level at 50 mV test potential. Blue lines indicate the zero current level. Inset to the lower right of panel shows voltage application protocol.

B. Tail current-voltage relationships for WT (open circles, n=7) and WT/G229D (filled circles, n=6). Tail current densities are plotted as a function of test potentials. Vertical lines for symbols indicate the standard error.

C. Current-voltage relationships for normalized tail curents in WT (open circles, n=7) and WT/G229D (filled circles, n=6). Vertical lines for symbols indicate the standard error.

Figure 5. ***Co-expression with G229D slows down the deactivation process.***

A. Current traces from CHO cells expressing WT (left) and WT/G229D (right). Currents were elicited by 2-s deperpolarizing-voltage step to 30 mV, followed by a reppolarization to −120 mV to obtain completely deactivated tail current. Blue lines indicate the zero current level. Inset to the lower right of panel shows voltage application protocol.

B. Bar graphs showing averaged tau_{fast} (left) , tau_{slow} (middle), and $A_{fast}/(A_{fast} + A_{slow})$ (right). White bars indicate data from WT (n=8) and black bars those from WT/G229D (n=10).

Figure 6.

(A-B) Atrial action potential-clamp recording.

A. Whole cell clamp was conducted by using an atrial action potential waveform (indicated in an inset below the traces). Representative two current traces recorded from cells expressing WT (black trace) and WT/G229D (red trace). Blue line indicates the zero current level.

B. Bar graph showing averaged integral current densities measured the area enclosed by the current curves. White bar indicates data from WT (n=10) and black bar indicates those from WT/G229D (n=11).

C. ***Resting membrane potential.***

Bar grahp showing averaged resting membrane potentials from CHO cells under four different conditions: no transfection of constructs (dot bar, n=23), transfected with WT (white bar, n=25), WT/G229D (black bar, n=15), and *KCNQ1*-G229D (strip bar, n=12). Blue line indicates the equilibrium potential of potassium ion in the present experimental condition.

Figure 7. ***Computer simulation study by employing both atrial and ventricular myocyte and 1D myocardial model.***

Numerically reproducedcurrent traces **(A)**, tail current-voltage relationships **(B)** and normalized activation curves **(C)** of WT model (open circles) and WT/G229D model (filled circles).

D. Atrial AP and I_{Ks} in the computer models of human atrial myocyte with WT-I_{Ks} or WT/G229D-I_{Ks}.

E. Ventricular AP and I_{Ks} in the computer models of human ventricular myocyte with WT-I_{Ks} or WT/G229D-I_{Ks}.

F. Transmural heterogeneity of AP and the simulated ECG in the 1D ventricular model.

Figure 1

A

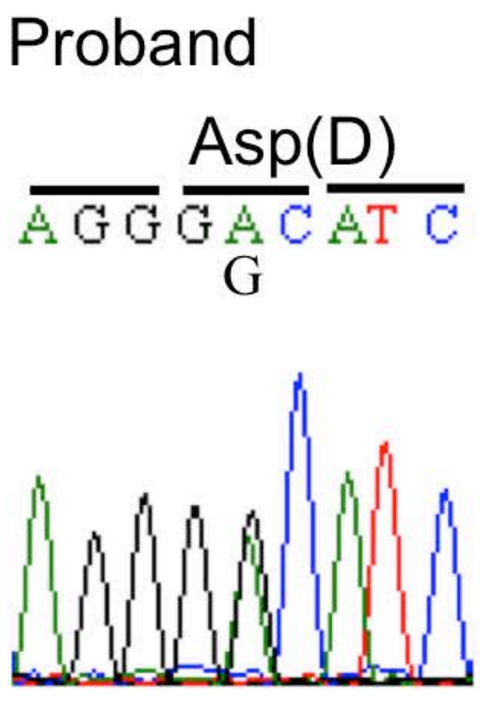
Proband
Asp(D)
A G G G A C A T C
G
Control
Gly(G)
A G G G G C A T C

B

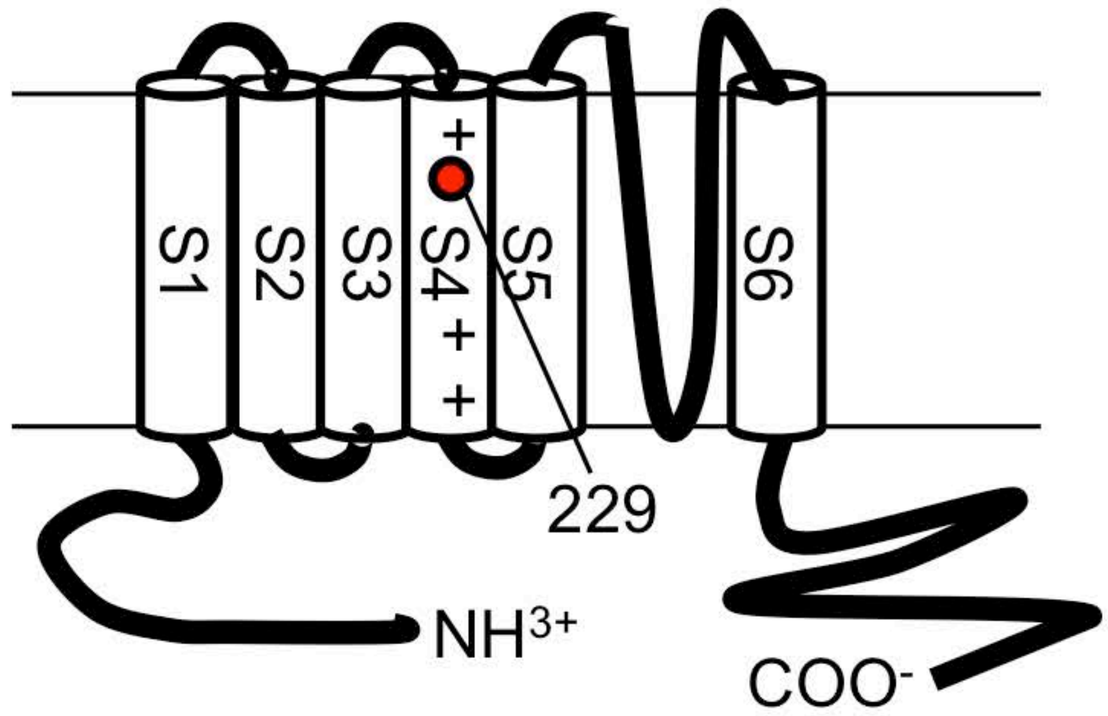
S1
S2
S3
S4
S5
S6
+
+
+
229
NH3+
COO-

C

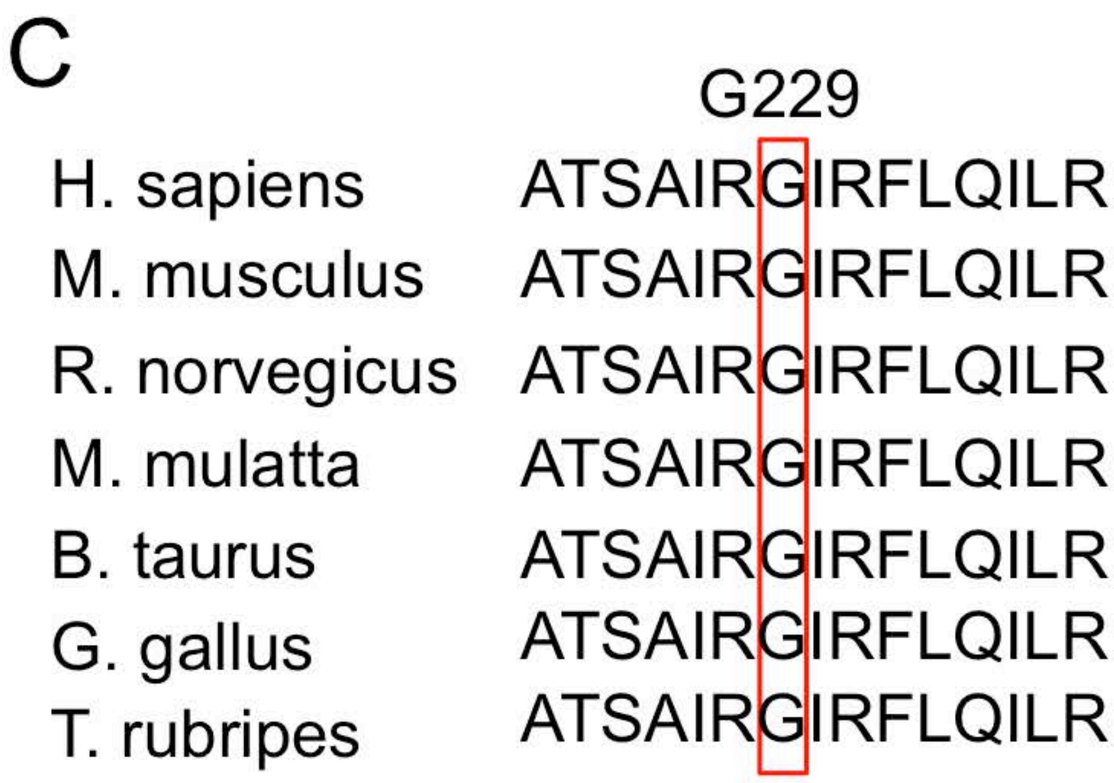
G229
H. sapiens ATSAIRGIRFLQILR
M. musculus ATSAIRGIRFLQILR
R. norvegicus ATSAIRGIRFLQILR
M. mulatta ATSAIRGIRFLQILR
B. taurus ATSAIRGIRFLQILR
G. gallus ATSAIRGIRFLQILR
T. rubripes ATSAIRGIRFLQILR

Figure 2

A

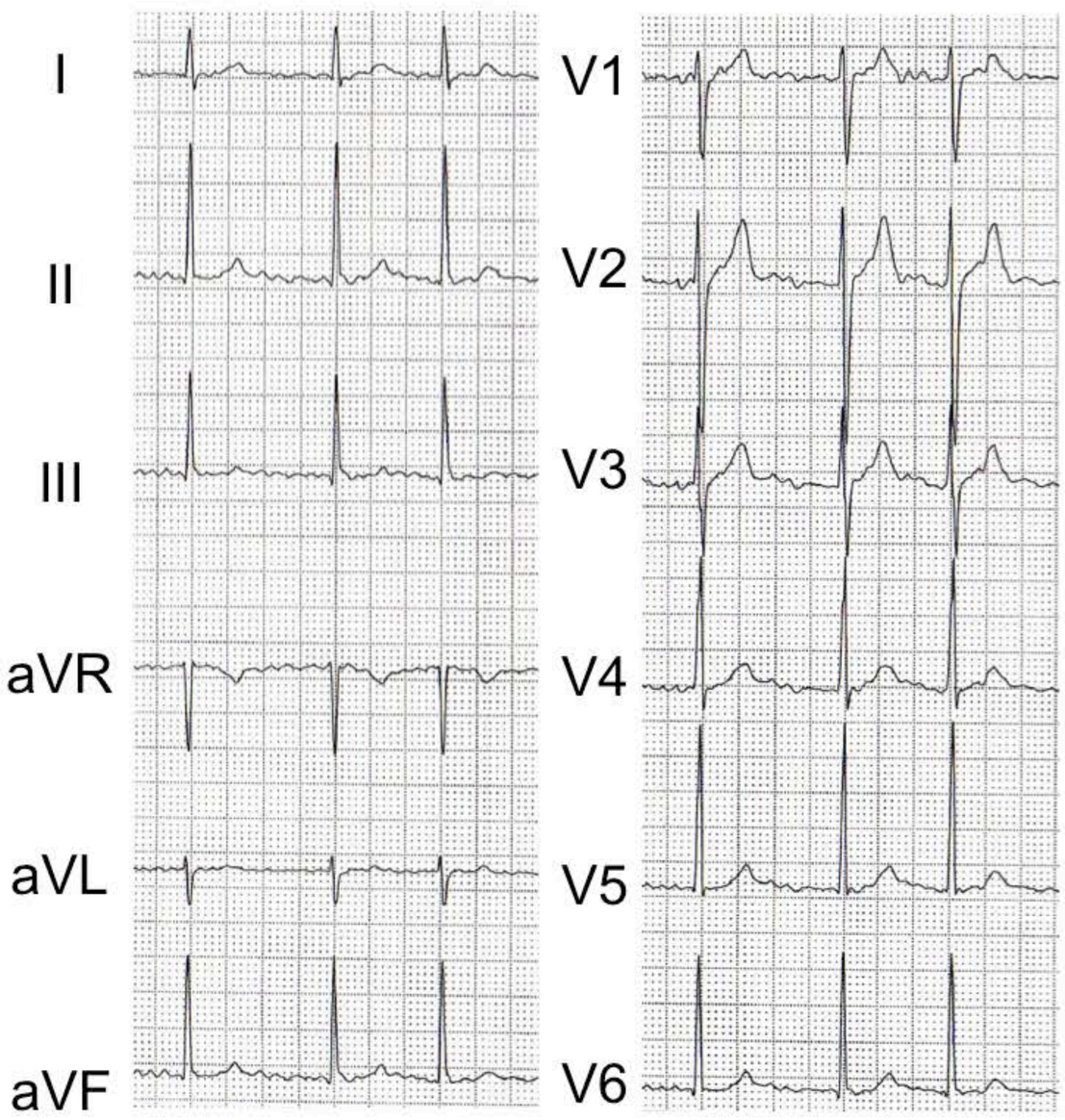

B

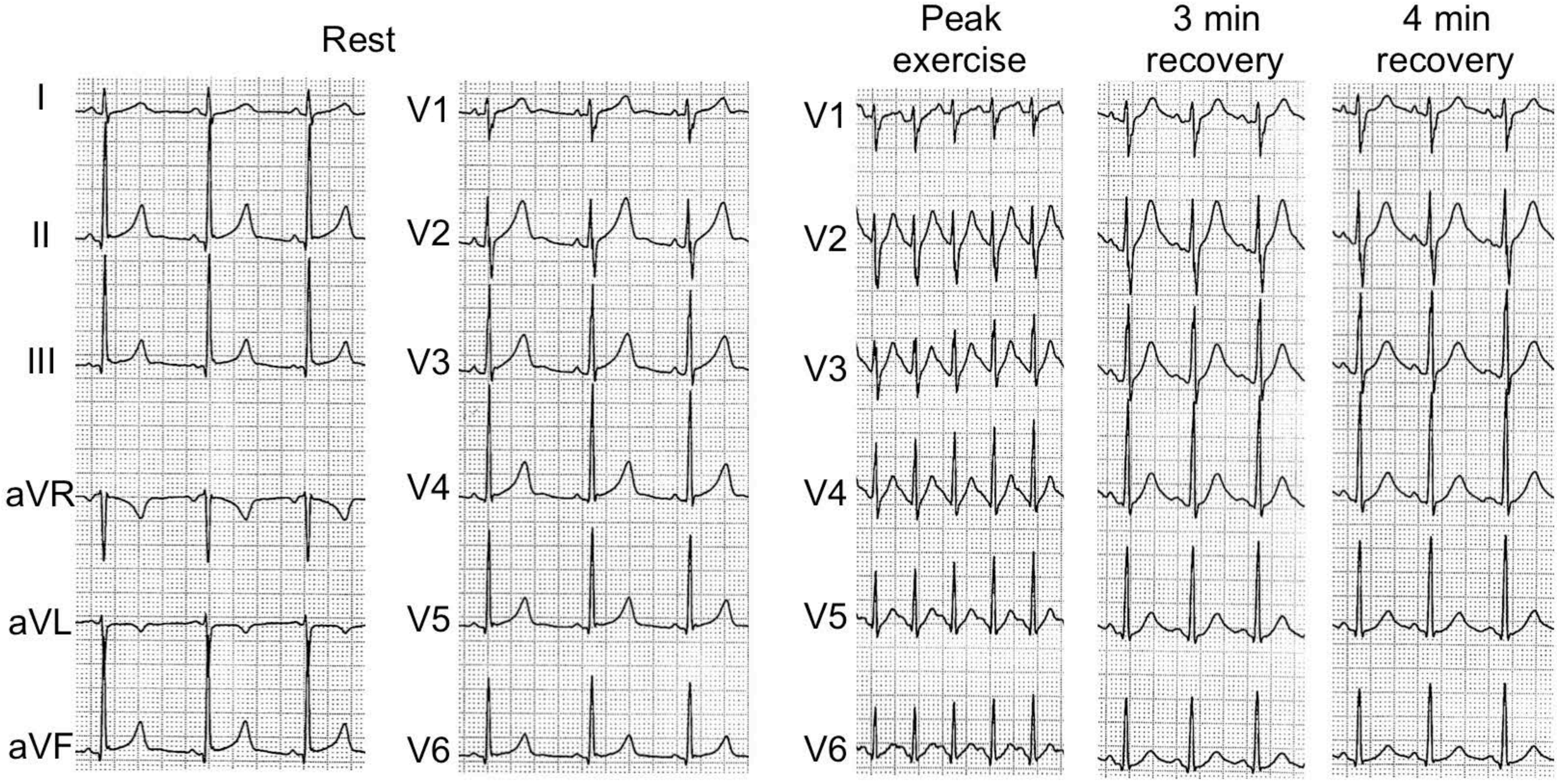

C

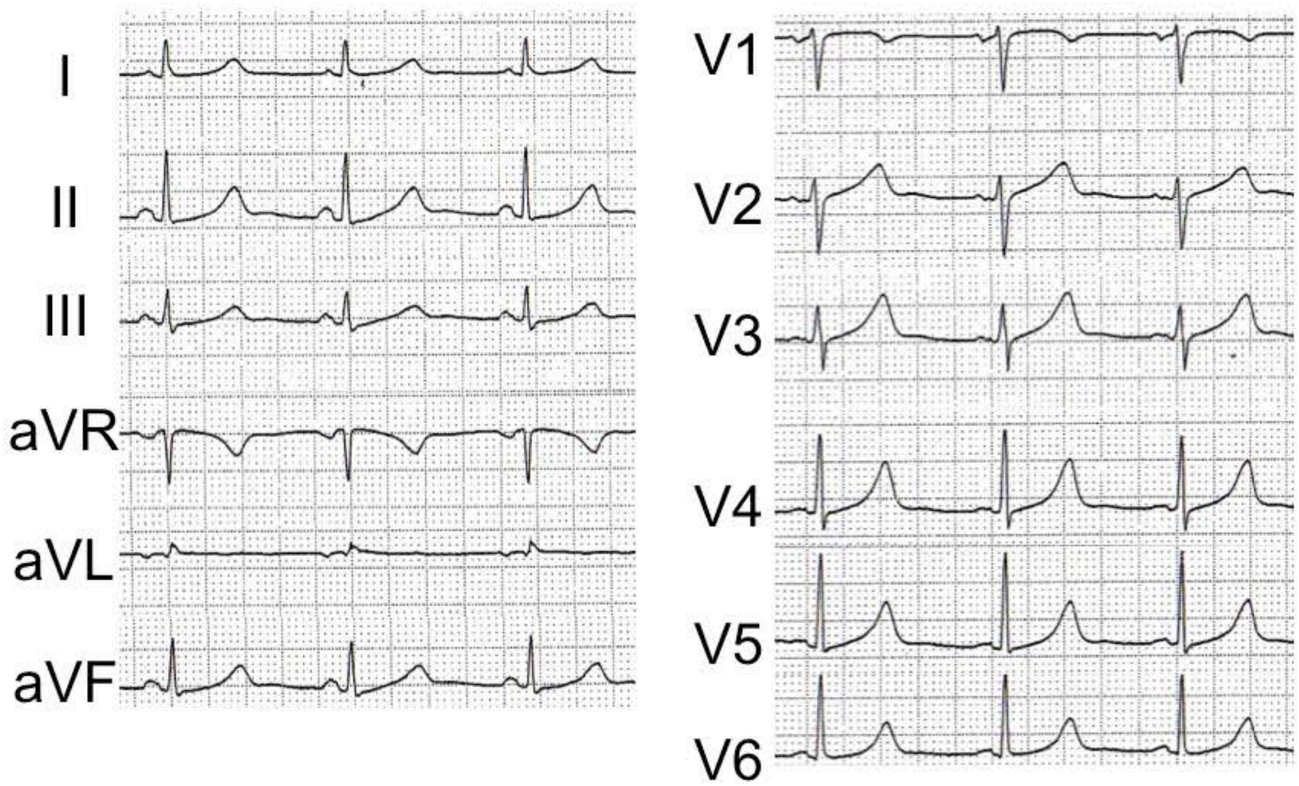

D

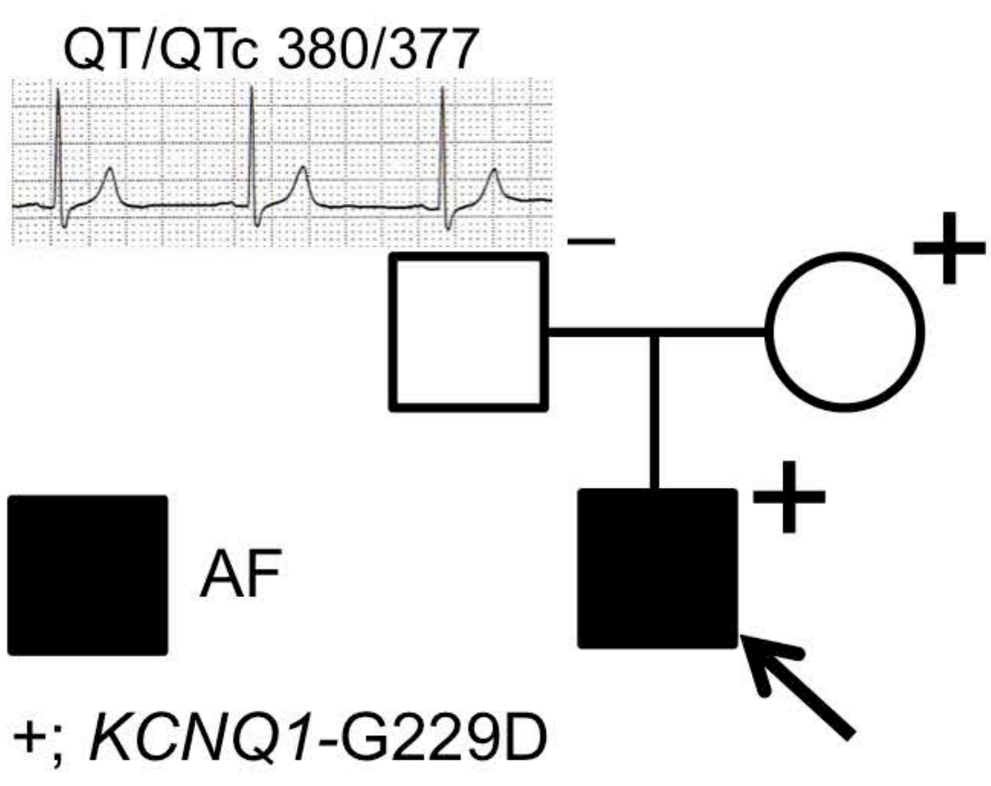

Figure 3

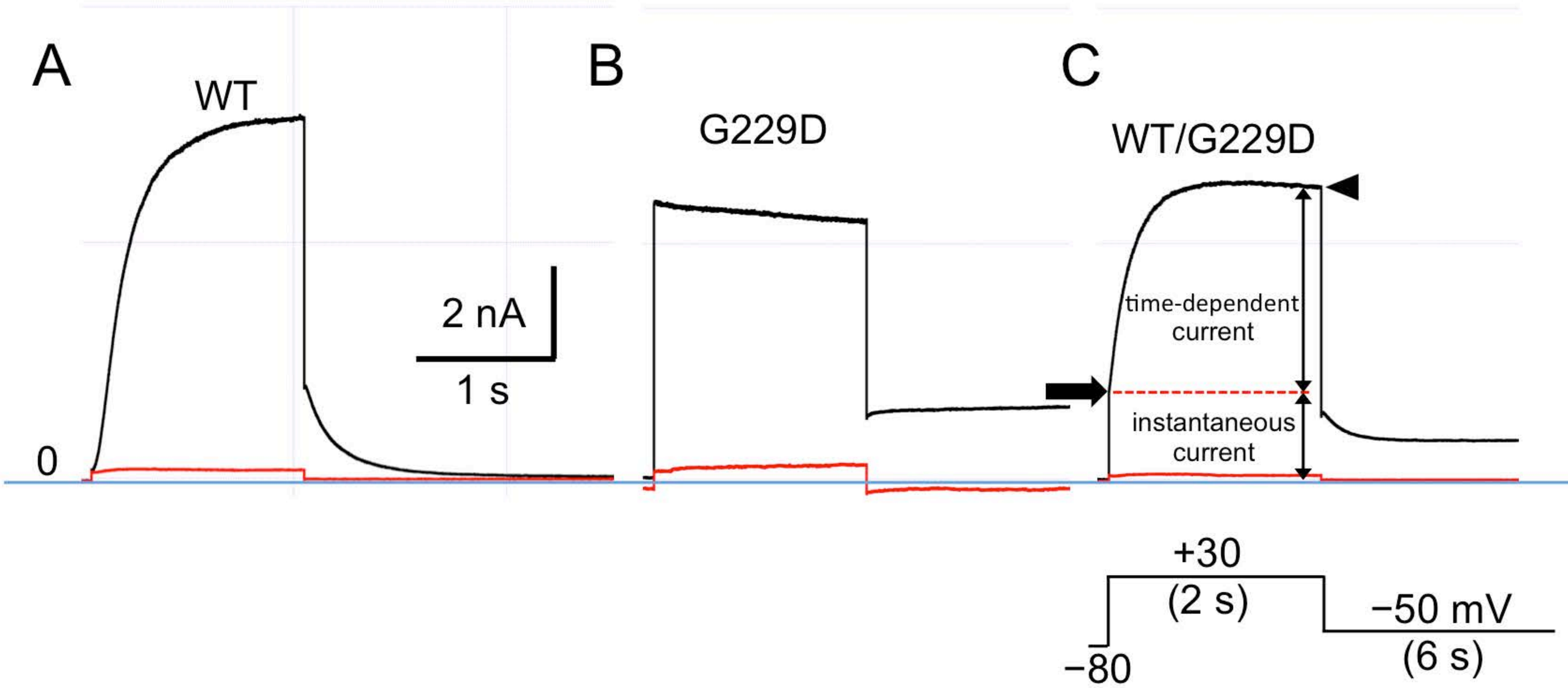
A
WT
2 nA
1 s
0
B
G229D
C
WT/G229D
time-dependent current
instantaneous current
+30
(2 s)
−50 mV
(6 s)
−80

D

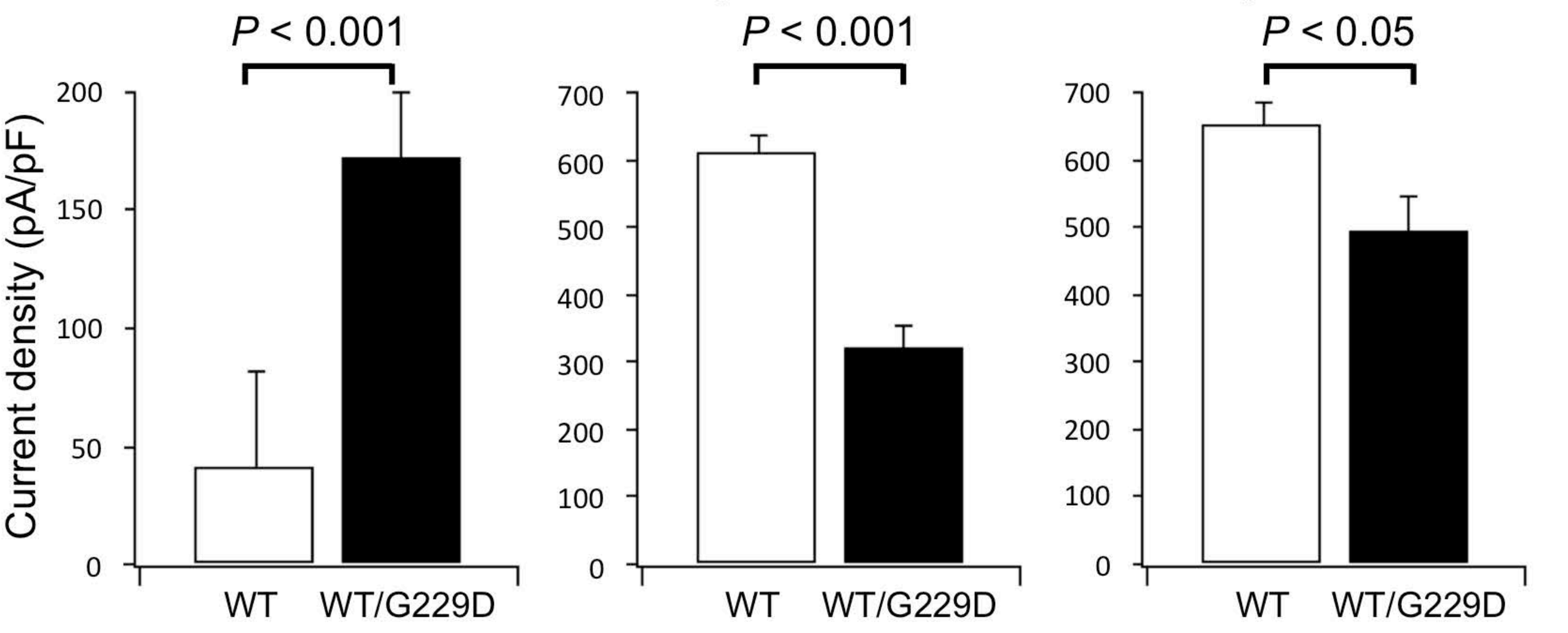
Instantaneous current
Time-dependent current
Steady-state current
P < 0.001
P < 0.001
P < 0.05
Current density (pA/pF)
200
150
100
50
0
700
600
500
400
300
200
100
0
WT
WT/G229D
WT
WT/G229D
WT
WT/G229D

Figure 4

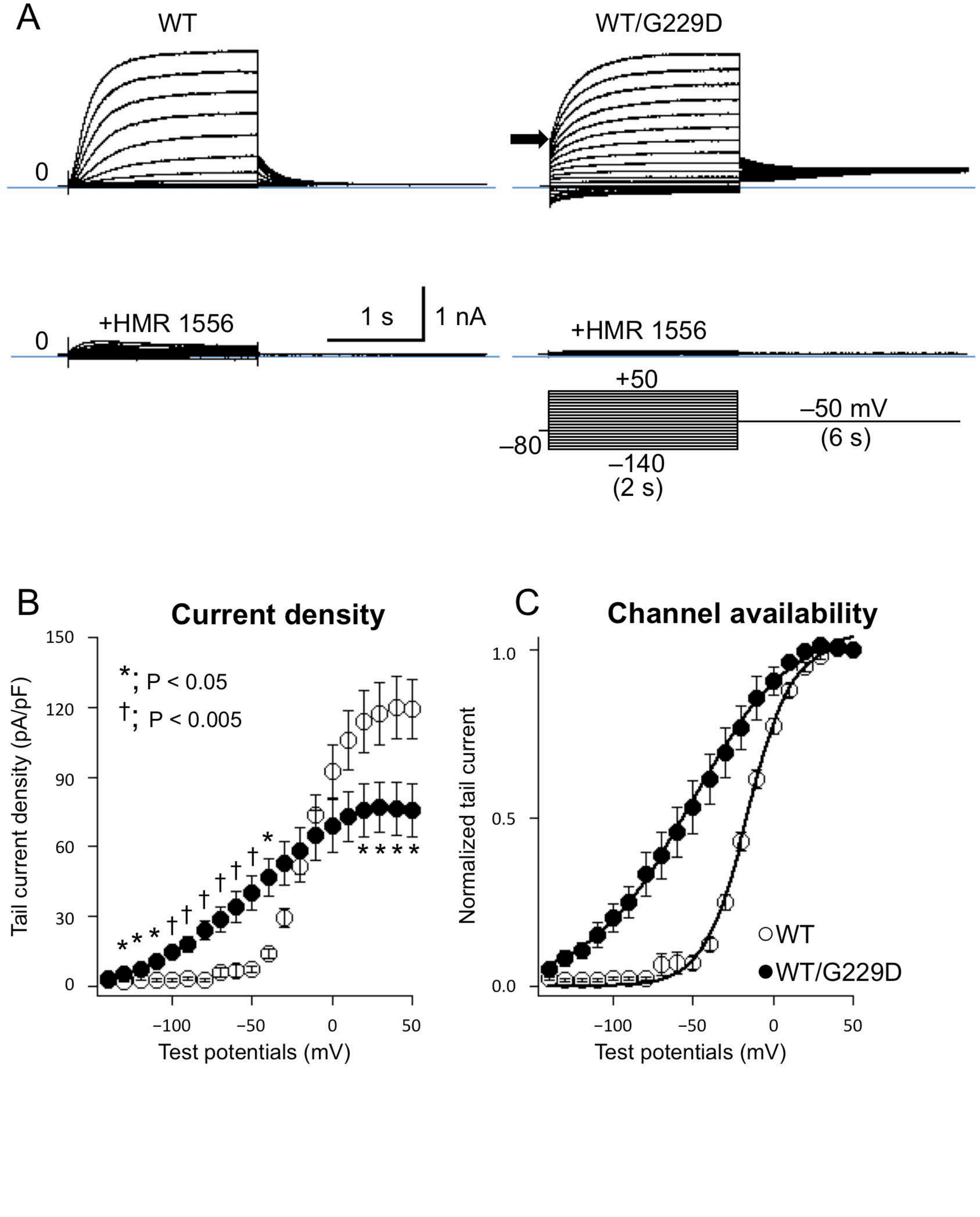
A
WT
WT/G229D
0
+HMR 1556
1 s
1 nA
0
+HMR 1556
+50
–50 mV
(6 s)
–80
–140
(2 s)
B
Current density
*; P < 0.05
†; P < 0.005
Tail current density (pA/pF)
150
120
90
60
30
0
−100
−50
0
50
Test potentials (mV)
C
Channel availability
Normalized tail current
1.0
0.5
0.0
−100
−50
0
50
Test potentials (mV)
WT
WT/G229D

Figure 5

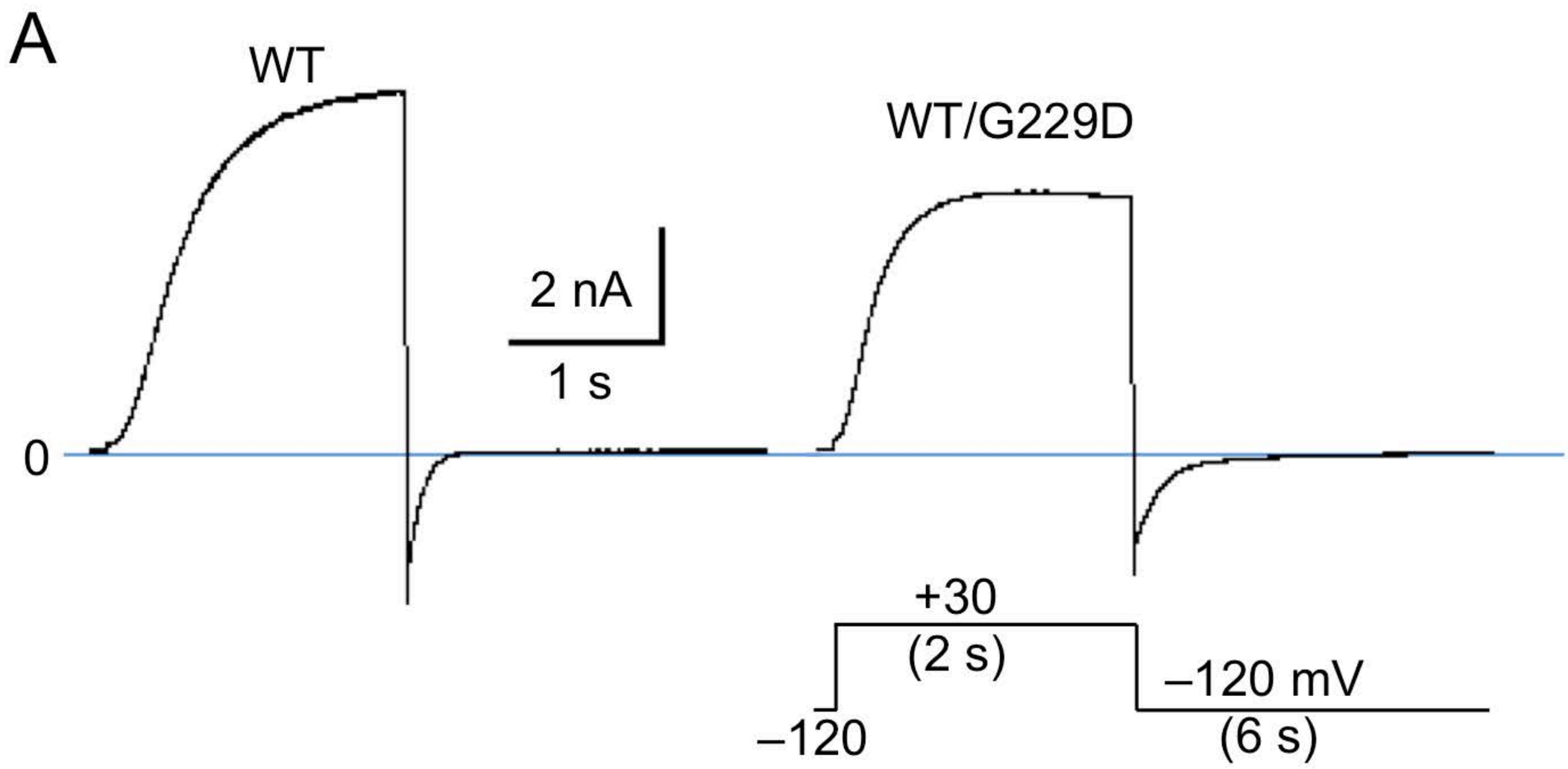
A
WT
WT/G229D
2 nA
1 s
0
+30
(2 s)
–120 mV
–120
(6 s)

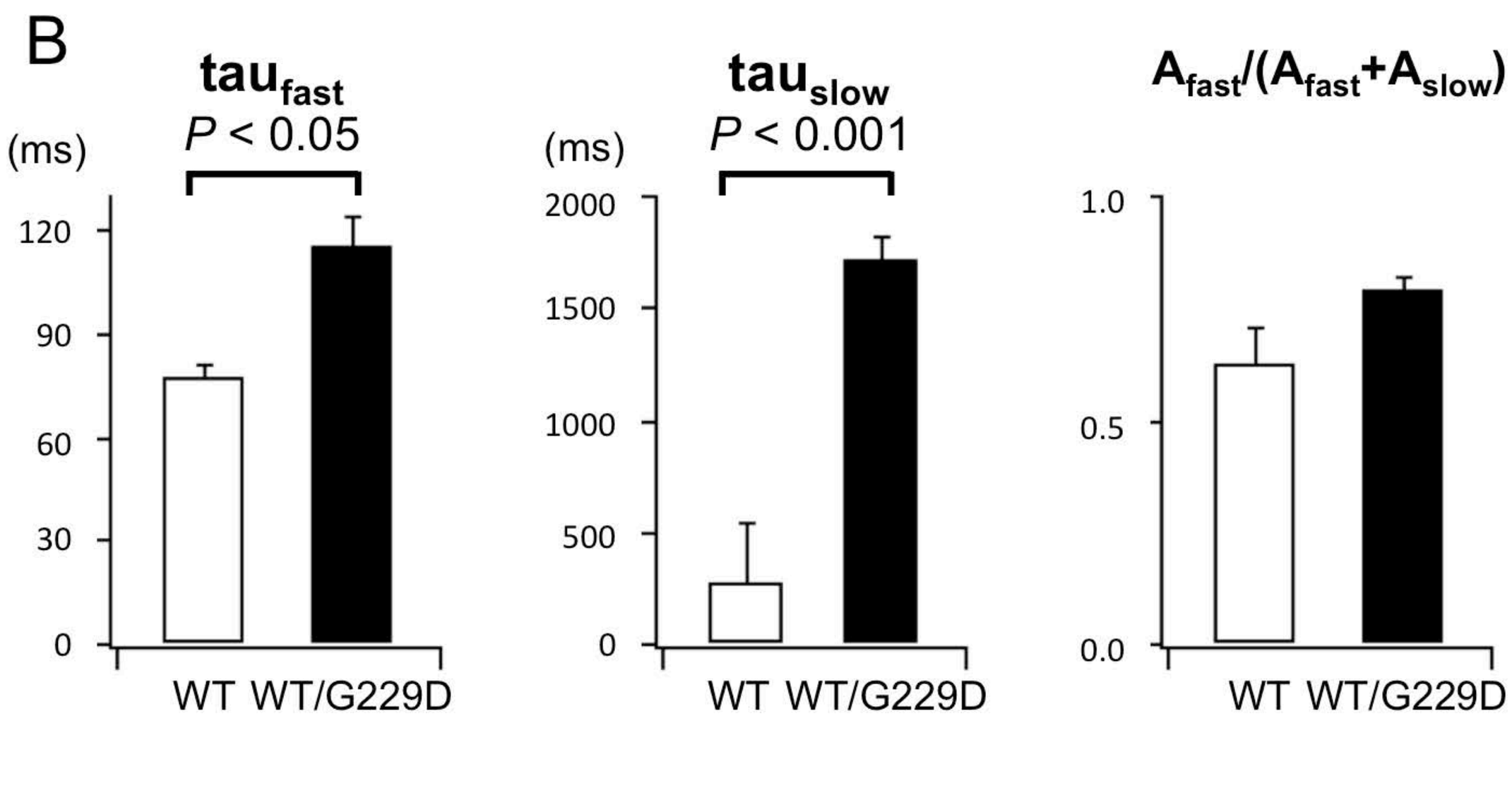
B
tau$_{fast}$
(ms)
P < 0.05
120
90
60
30
0
WT WT/G229D
tau$_{slow}$
(ms)
P < 0.001
2000
1500
1000
500
0
WT WT/G229D
A$_{fast}$/(A$_{fast}$+A$_{slow}$)
1.0
0.5
0.0
WT WT/G229D

Figure 6

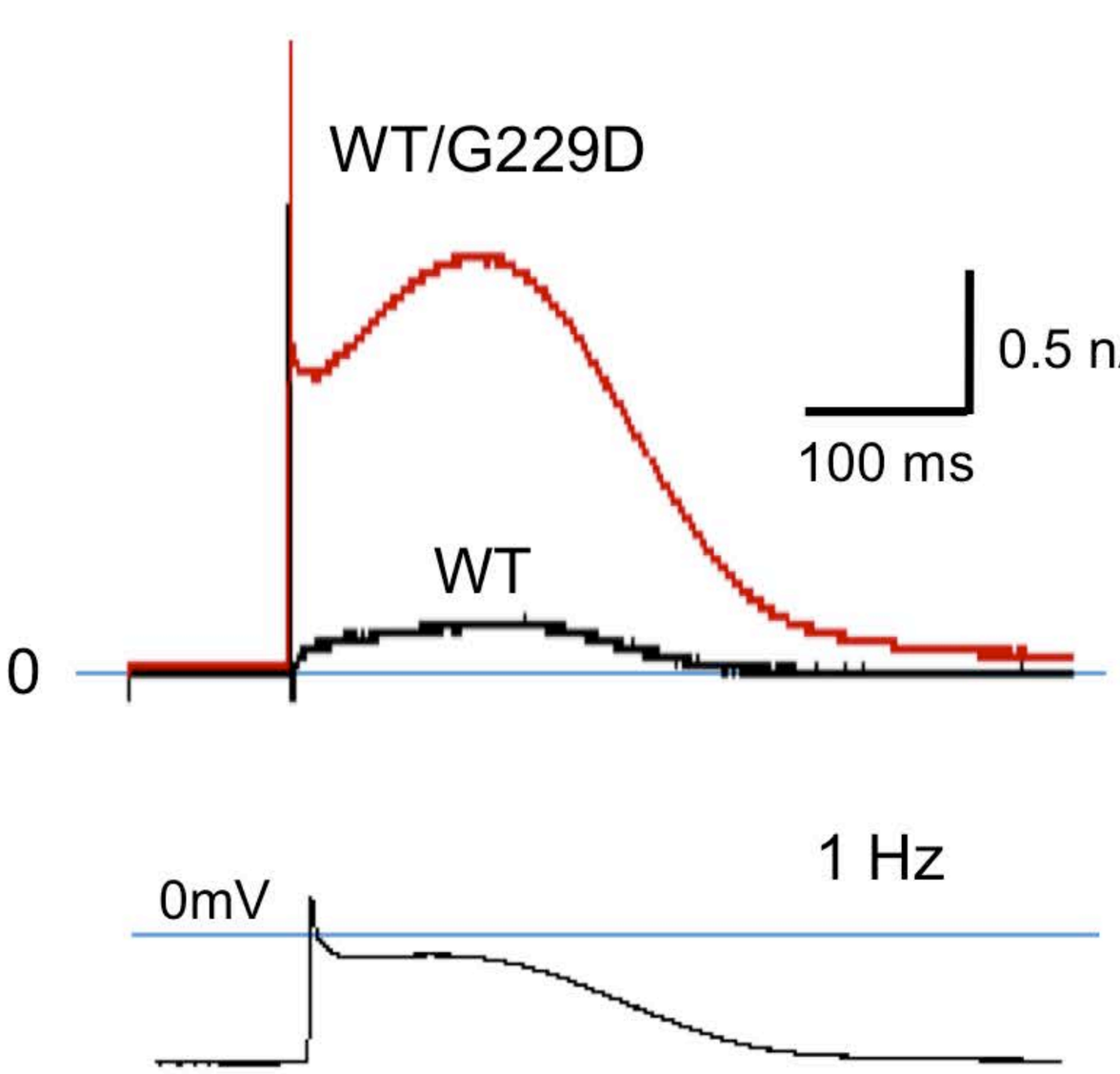
A
WT/G229D
0.5 nA
100 ms
WT
0
1 Hz
0mV

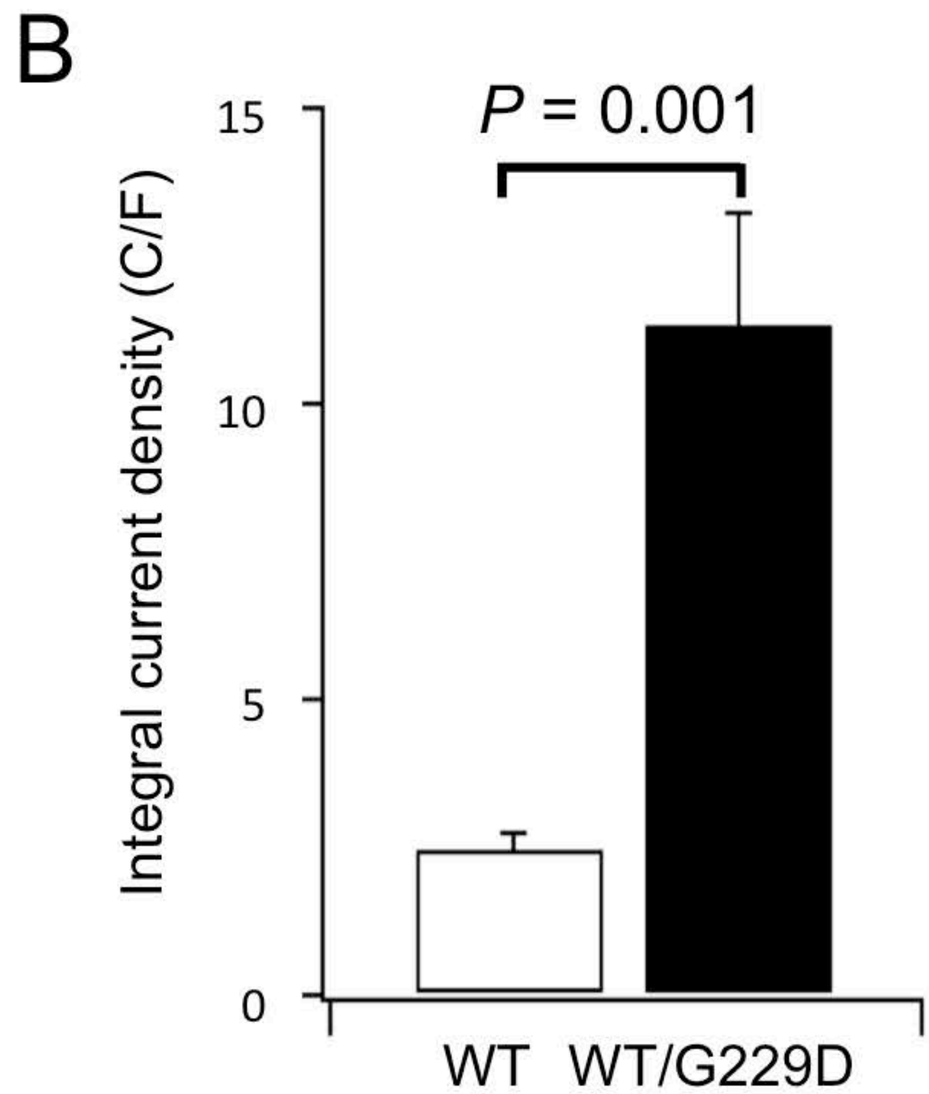
B
P = 0.001
Integral current density (C/F)
15
10
5
0
WT
WT/G229D

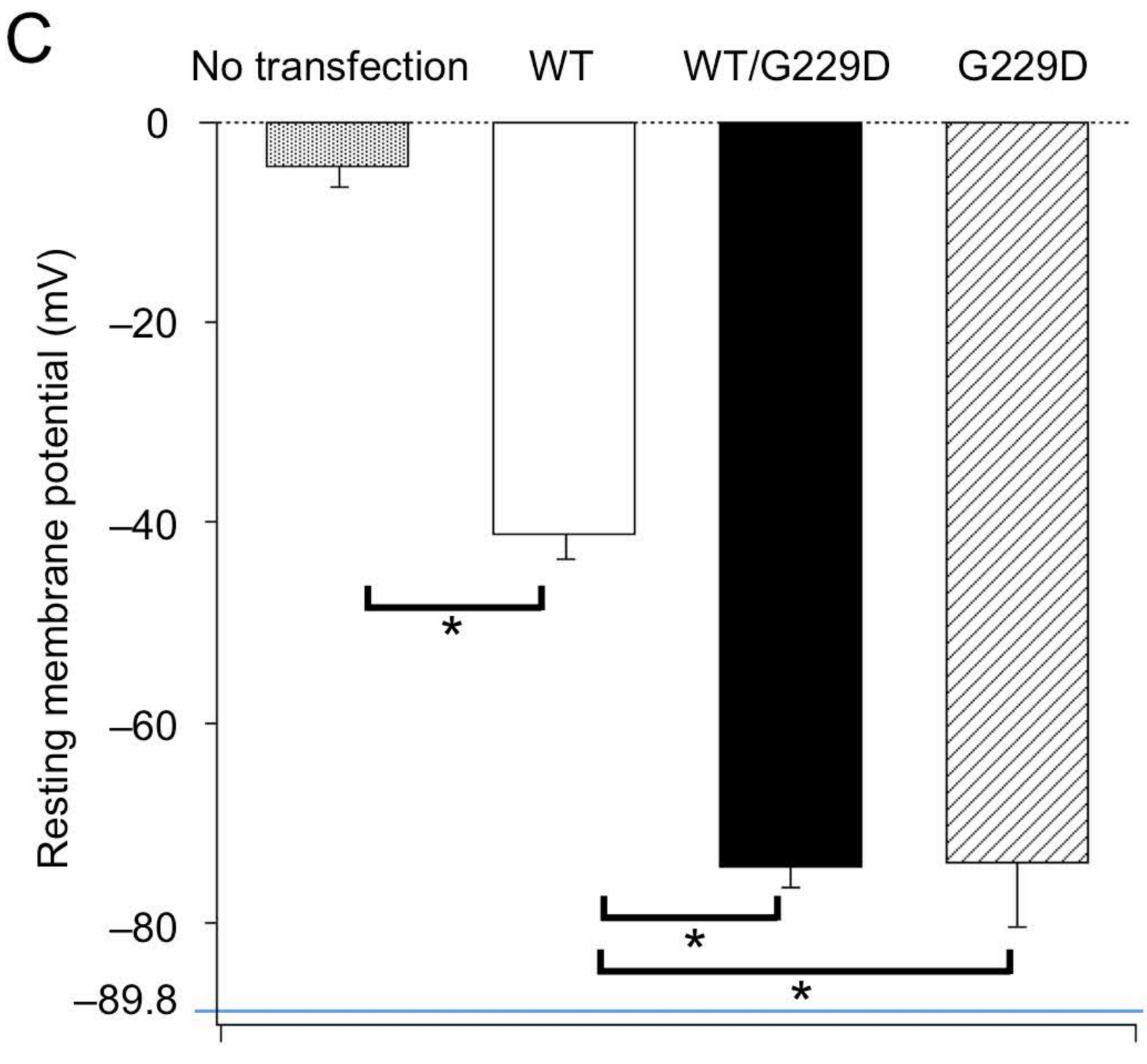
C
No transfection
WT
WT/G229D
G229D
Resting membrane potential (mV)
0
–20
–40
–60
–80
–89.8
*
*
*
*; P < 0.001

A

WT

0.2 pA/pF

1 s

WT/G229D

B

WT

WT/G229D

Tail current density (pA/pF)

0.15
0.12
0.09
0.06
0.03
0

–100 –50 0 50

Test potentials (mV)

C

Normalized tail current

1.0
0.5
0.0

–100 –50 0 50

Test potentials (mV)

D

WT

WT/G229D

1 Hz

200 ms

V_m

(mV)
30
0
–30
–60
–90

APD_{90} 294 ms

APD_{90} 232 ms

I_{Ks}

0.4
0.3
0.2
0.1
0
(pA/pF)

E

WT

WT/G229D

1 Hz

200 ms

APD_{90} 263 ms

APD_{90} 254 ms

0.15
0.1
0.05
0
(pA/pF)

F

WT

WT/G229D

Pacing (1 Hz)

Endo 0.06

M 0.6

Epi 0.24 (cm)

2 cm

ECG Recording Electrode

t

200 ms

30
0
–30
–60
–90
(mV)

V_m (mV)

50
0
–50
–100

M

Endo

Epi

Simulated ECG

QT = 404 ms

QT = 402ms

Figure 7